JGR Solid Earth

RESEARCH ARTICLE
10.1029/2020JB019917

Constraining Internal States in Progressive Rock Failure of Carrara Marble by Measuring Residual Strains With Neutron Diffraction

A. Voigtländer[1,2], K. Leith[3], J. M. Walter[4], and M. Krautblatter[1]

[1]Landslide Research Group, Technical University of Munich, Munich, Germany, [2]Helmholtz Centre Potsdam, GFZ German Research Centre for Geosciences, Potsdam, Germany, [3]Department of Earth Sciences, ETH Zurich, Zurich, Switzerland, [4]Geoscience Center, University of Göttingen, Göttingen, Germany

Key Points:
- Neutron diffraction techniques allow nondestructive assessment of internal strain states of rocks
- Inherited residual strain state of Carrara marble is overall contractional
- Residual strain is indicative of the strength and possible damage state of rocks

Supporting Information:
- Supporting Information S1

Correspondence to:
A. Voigtländer,
anne.voigtlaender@gfz-potsdam.de

Citation:
Voigtländer, A., Leith, K., Walter, J. M., & Krautblatter, M. (2020). Constraining internal states in progressive rock failure of Carrara marble by measuring residual strains with neutron diffraction. *Journal of Geophysical Research: Solid Earth*, *125*, e2020JB019917. https://doi.org/10.1029/2020JB019917

Received 4 APR 2020
Accepted 19 MAY 2020
Accepted article online 23 MAY 2020

Abstract Knowledge of the internal state of rock is key to anticipate its rheological response and susceptibility to external factors. Time-dependent failure in rock is controlled by internal state changes, like damage accumulation or strength degradation. But assessing internal states and changes thereof, nondestructively and independent of external forcing is not straightforward. Residual strains, measured with neutron diffraction techniques are used as a proxy for the internal state in material sciences. We investigated its potential for progressive rock failure by measuring residual strain states of an untested and three mechanically and chemomechanically pretested Carrara marble samples. We collected neutron diffraction data for three crystal lattice planes $\{10\bar{1}4\}$, {0006}, and $\{1\bar{1}20\}$. Measurements showed an initial overall contractional spatially homogeneous residual unit cell volume strain state of about −400 μstrain, though magnitudes were strongly partitioned among measured crystal lattice planes. However, they are equal within the spatial orientations of the intact sample. For the pretested samples, the induction and relaxation of strains varied spatially with the pretesting stress field and environmental conditions. The vertical extent of superposition of the initial residual strain state was greatest in wet samples, the magnitude of induced extensional strain highest in the dry sample. This indicates chemomechanically enhanced subcritical crack growth with concomitant residual strain relaxation as well as the mitigation of extensional strain built up by the presence of water during pretesting. Our experiments show that residual strain has a significant potential to provide insights into past and actual internal states to anticipate progressive rock failure.

1. Introduction

The failure of rocks impacts the face of the Earth by driving landscape evolution, limiting infrastructure performance, and causing natural hazards. While in brittle rock, failure proceeds in a progressive manner, where microscopic, subcritical damage extends over time and eventually leads to critical deformation and macroscopic failure, the capability to anticipate their evolution is still restricted. This is partially due to methodological limitations to gain direct and nondestructive insight into material states, and few experimental studies on the accommodation of subcritical deformation and damage at the grain scale. Conventionally, rheological characterization of rocks relies on destructive tests that measure the divergence from an initial state (Brantut et al., 2012, 2014; Diederichs, 2003; Eberhardt et al., 1999). These experiments are generally restricted to measure whole-rock-sample properties, like strength and deformation, and are not designed to determine a preexisting initial state independent of external forcing (Covey-Crump & Schofield, 2009; Schofield et al., 2003, 2006). In material sciences, focusing on long-term strength, toughness, and performance of engineered materials, thus material properties in resistance to progressive failure, methods, and mechanistic concepts have been established to assess the internal state of the materials and changes thereof (Ritchie, 2011; Withers, 2015). Residual elastic strains, measured with diffraction techniques are used as a proxy for the internal state in material sciences. With the concept of residual elastic strains, in short, residual strains, internal states, and rheology of engineered materials can be described (Withers & Bhadeshia, 2001a, 2001b). Here, we apply the concept of residual strain to natural rocks and measure those with neutron diffraction to better understand their internal state and progressive failure.

Rocks are subject to stresses throughout their geologic lifespan. As they exhume, both imposed confinement and ambient temperatures reduce and introduce differential stresses (Zang & Stephansson, 2010). During exhumation and the accompanied unloading, not all of the induced elastic strain energy is released. Strains that remain in a rock in the absence of boundary loads are referred to as "residual" (Voight, 1966). Residual strains equilibrate globally but can vary locally at the grain scale (Friedman, 1972). Residual stresses or strains in rocks may result from thermal- or mechanical-induced purely elastic processes, inelastic yielding, or a combination of both (Holzhausen & Johnson, 1979). Permanent deformation locks-in elastic strains within the rock, similar to tempered glass. Elastic distortions could also be locked in by internal self-constraint of neighboring crystallites and their crystallographic geometry (Meredith et al., 2001). Emery (1964, p. 244) stated, therefore, that "[...] any rock, because it is a rock, must have in it more or less conserved elastic strain energy and that its present condition is a transient one and represents the sum of all that has happened to the rock." Since then, studies have reported residual strain in rocks indicating grain-scale strain magnitudes in the order of $\times 10^{-3}$ μstrain (Friedman, 1972; Siegesmund, Mosch, et al., 2008). In geological materials, unlike for engineered materials, stress conditions and magnitudes of external forces which were necessary to produce the observed residual strains are unknown. The residual strain state has, therefore, itself been widely used to infer the stress magnitude and spatial direction of former geological stress fields (Engelder & Sbar, 1977; Sekine & Hayashi, 2009; Zang & Berckhemer, 1989).

Residual strains also affect the rheology of rock (Holzhausen & Johnson, 1979; Voight, 1966). It is currently reasoned that the strain magnitude and sign reflect the interatomic spacing, spatial array of atoms in the individual crystal lattices, and their energetic states (Withers & Bhadeshia, 2001b). The amount of compressive stress that atomic bonds can repulse before breaking, defines the maximum compressive strength of the crystal and is consequently related to the polycrystalline strength. Likewise, the amount of tensile stress a bond can support defines the maximum tensile strength of the material. The strain state of crystal lattice planes strongly defines the possible response of rocks to applied external forces, including bulk fracture toughness or strength. Next to the influence of residual stresses and strains on rock deformation, externally applied forces can relax preexisting as well as induce new strains.

In general, it is assumed that stored strains can be relaxed when grains or crystals are freed from the neighboring constraints (Friedman, 1972). This can be achieved by the opening of microcracks and also by grain boundary glides and chemically altered grain boundary cohesion (Engelder et al., 1977; Luzin et al., 2014; Silberberg & Hennenberg, 1984). Spatial direction and relative magnitudes of residual strains are controlled by the presence of microcracks created by tectonic stresses, stress relief, and weathering, which in turn influences the mechanical strength of rock (Hoskins & Russell, 1981). Externally applied stresses causing any local permanent deformation, by distortion of crystal structure, chemical cementation, or thermal recrystallization could lock-in elastic strains which would overprint preexisting residual strains (Friedman, 1972; Holzhausen & Johnson, 1979; Withers & Bhadeshia, 2001b). The introduction of residual strains is not necessarily spatially uniform (Figures 1a and 1b) due to (i) heterogeneous yielding and stress concentrations at microstructural flaws, (ii) anisotropic thermal expansion coefficients, and (iii) mechanical or thermal stress gradients (Holzhausen & Johnson, 1979; Timoshenko & Goodier, 1970). Likewise, the relaxation of residual strains is spatially variable (Nichols, 1975). Internal damage state relevant for progressive rock failure occurs due to both, the formation of cracks (i.e., strain relief) and the inducement of especially extensional elastic strain.

In engineered materials not only the effect of mechanical stresses on residual strain is investigated but also environmental conditions. Physical and chemical weathering cause alteration of material properties, including stiffness, and can enhance subcritical crack growth (Atkinson & Meredith, 1987; Nara et al., 2017; Peck, 1983). Residual strain response and deformation mechanisms to thermally induced stresses have been determined in geologic materials (Luzin et al., 2014; Meredith et al., 2001; Siegesmund, Mosch, et al., 2008). However, the effect of moisture or chemically enhanced mechanisms, have only been reported for metals and engineered materials. Here, residual strains pose a first-order control on chemically enhanced subcritical crack growth, referred to as stress corrosion (King et al., 2008; Toribio, 1998). The effect of residual strains on stress corrosion cracking in rocks has been postulated but has not been investigated (Atkinson & Meredith, 1987).

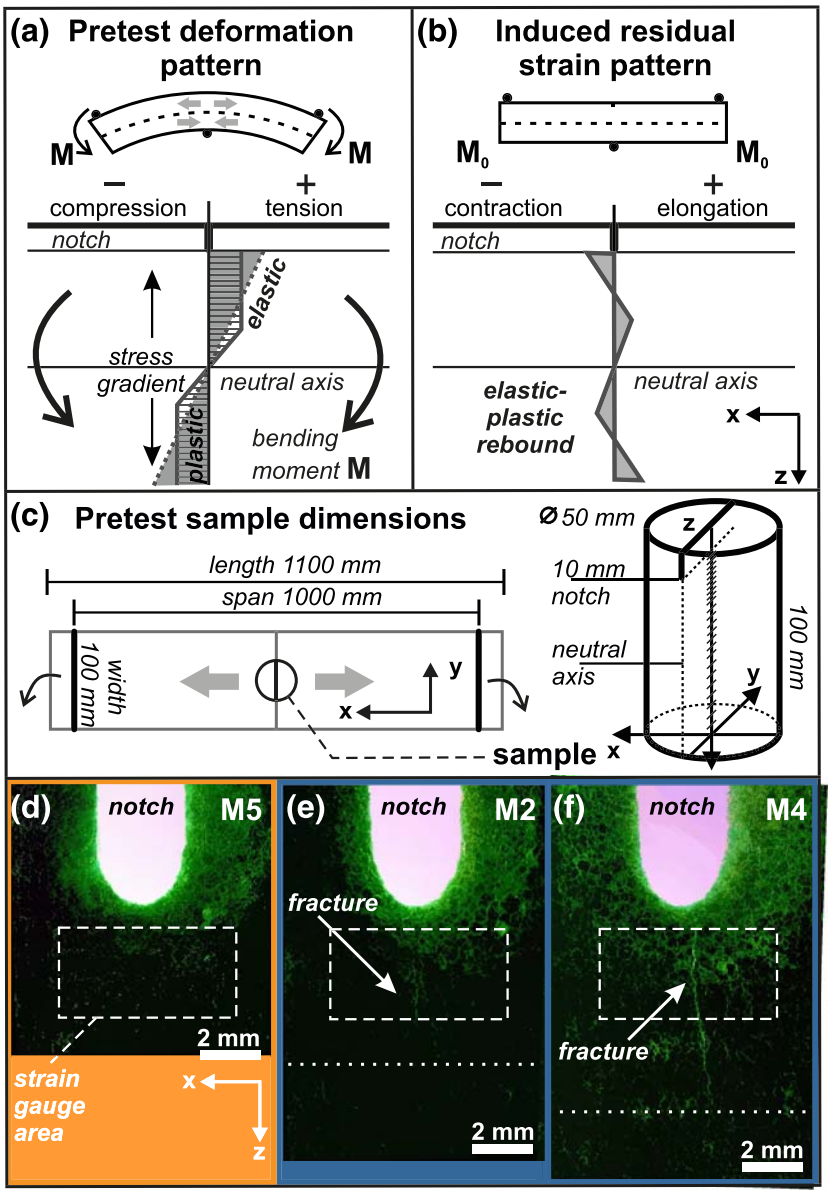

Figure 1. (a) Schematic pretest deformation pattern, (b) resulting induced global residual strain state without brittle fracturing. (c) Pretest and measured sample dimensions, direction, and measurement point distribution along the vertical axis. Fluorescent dyed thin section image of the notch area of (d) sample M5, pretested with dry condition at the notch, (e and f) sample M2 and M4, pretested with wet condition at the notch. The extent of localized fractures is indicated by a dotted line. The dashed area highlights the position of strain gauge measurements during the pretest.

Initially, so-called "residual stresses" (measured as residual strains) have been examined using strain relief methods including overcoring, microcrack orientation, and density maps (Hoskins & Russell, 1981; Zang & Berckhemer, 1989). Likewise, in conceptual approaches, residual stresses have been linked to rock failure, exfoliation and spalling (Emery, 1964; Kieslinger, 1958; Müller, 1969). Hereby, instantaneous or time-dependent inelastic subcritical damage is assumed to decrease strain magnitudes. These destructive and invasive methods measure bulk strains on the surface of rock samples. As the relaxation of the residual strains is assumed to be achieved by the creation of new surfaces, these microcracks can then be evaluated in thin sections. In contrast to this, neutron diffraction techniques enable the nondestructive measurement of residual strain in the interior of solid polycrystalline rock materials (Holden et al., 1995; Schofield et al., 2006; Withers & Bhadeshia, 2001a). Deviations in lattice parameters can be quantified and subsequently elastic

strain, microstructural properties, and damage can be derived. Neutron diffraction allows assessing elastic strains at the grain-scale on conventionally sized samples (Hall et al., 2011; Schofield et al., 2006). These methods enable us to explore phenomena such as subcritical crack growth and creep, where deformation-induced microstructural and strain change are expected to be small and to assess the spatial variability of strain change within the rock sample.

Advancing possibilities and especially in situ testing have increased the application of neutron diffraction in rock physics, for rock mechanical problems and by providing data for numerical models. However, for time-dependent rock deformation experiments, in situ testing is not applicable due to time constraints at research reactors, and testing environments are generally limited to thermal experiments, as water absorbs neutrons. To assess time-dependent rock deformation and wet conditions with regard to internal strain states that we simplified the problem: We (i) focused on a well-studied Carrara marble, a homogeneous and monomineralic metamorphic rock, and (ii) used mechanically or chemomechanically pretested samples to evaluate different altered states. Neutron diffraction data were collected of an intact sample and three mechanically and chemomechanically pretested samples, assuming that the initial residual strain state is similar in all samples, enabling their comparison. With these data we (i) defined the initial residual strain state of Carrara marble, (ii) assessed the inducement of strains due to the mechanical pretesting, and (iii) inferred the role of the internal (i.e., initial residual strain) and external (i.e., subcritical mechanical loading and dry and wet testing conditions) factors on the induced damage extent. By comparing the relative effect of external and internal factors, our study provides novel insights into the role of residual strains on progressive rock failure.

2. Material Characterizations and Methods

Here we report on the essential characteristics of the material and the pretesting with regard to the applied neutron diffraction techniques. The main characteristics of the used Carrara marble (section 2.1), and the sample preparation, pretest setup, and observations (section 2.2) are given. Details on both were reported and discussed by Voigtländer et al. (2018). In section 2.3 we introduce the applied neutron diffraction technique and describe the measurement procedure applied in this study (section 2.4).

2.1. Carrara Marble

The Carrara marble used, consisted of monomineralic calcite (>98% $CaCO_3$) with a mean grain size of ~200 μm and a dry density of ~2.7–2.8 g/cm^3. The polycrystalline metamorphic rock samples display a near-random crystallographic preferred orientation (CPO) and are therefore regarded as texturally nearly isotropic (Voigtländer et al., 2018, Figure S1).

Distinctive diffraction patterns are formed due to the trigonal crystal structure of calcite (unit cell dimensions and axis: $a = b \neq c$, $\alpha = \beta = 120°$, $\gamma = 90°$, $a \approx 4.9887$ Å, $c \approx 17.0623$ Å; Rao et al., 1968). These characteristics facilitated repeatable mechanical testing and relatively unambiguous neutron diffraction patterns. Previous neutron diffraction measurements on Carrara marbles have affirmed the presence of residual strains within in the order of –400 μstrains due to their metamorphic history (Scheffzük et al., 2007).

2.2. Sample Preparation to Induce Residual Strain and Damage States

To obtain mechanically and chemomechanically altered states of Carrara marble we pretested samples under dry and wet conditions previously described in Voigtländer et al. (2018). These pretests consisted of inverted single-edge notch three-point (iSENB) bending creep tests on Carrara marble beams (Figure 1a). All samples were cut from the same block. Samples dimension were 1,100 mm × 100 mm × 100 mm with a 10 mm notch in the center (Figure 1c). The principal longitudinal stress direction was in the x direction of the sample. Due to the loading configuration, the induced stress state was graded along the vertical axis (z direction) as the stress shifts from tension in the upper half to compressive stresses in the lower half of the beam (Figure 1a). Macroscopic surface deformation in the axial direction was monitored with strain gauges at the notch tips during the pretesting (Figures 1d–1f, Voigtländer et al., 2018). Carrara marble samples, M2, M4, and M5 used for this study, were mechanically loaded in two stages, with dead weight loads calculated for the initial sample geometry and percentage wet fracture toughness (K_{IC}, ~1.3 MPa/m$^{1/2}$, Voigtländer et al., 2018). First, the three samples (M2, M4, and M5) were loaded to ~55% K_{IC}. In a second step, loads were raised to ~77% K_{IC} in M5 and M2 (subsequently increased to ~80% K_{IC}) and to ~85% K_{IC}

in M4. Throughout the testing period, calcite-saturated water was added to the notch of samples M2 and M4, while M5 remained dry, at ambient temperature and humidity.

Because these samples were to be used in this study on the internal states, they were only allowed to creep but not to fail. We had no criterion when that would happen. Experiments showed that, as soon as tertiary creep was reached, failure of the samples could not be prevented. This was (i) due to our simple dead weight loading system and (ii) the speed of dynamic fracturing. To prevent this, we unloaded the samples when the strain rates at the notch tip increased by an order of magnitude and we assumed that tertiary creep was being approached. This was the case for samples M2 and M4, with wet condition at the notch loaded to ≥80% K_{IC} after 27, respectively 25 days in the pretest. Dry samples in the same testing configuration did not approach tertiary creep during testing periods even at loads of ~85% K_{IC} unless water was introduced to the notch. Possible chemomechanical effect leading to these behaviors are discussed in Voigtländer et al. (2018) and references therein. M5, the dry pretested case was unloaded at the termination of the testing period after 48 days. Figure 1d–1f are fluorescent-dyed thin section images of the notch areas of samples M5, M2, and M4, highlighting the microstructurally visible damage induced during the pretest. Thin sections of samples tested with water present at the notch (Figures 1e and 1f) revealed single localized fractures along grain boundaries. No induced fracture was observed in the thin section of sample M5 (Figure 1d).

Cylindrical subsamples ($ø = 50$ mm, $h = 100$ mm) were cored vertically through the center of samples M5, M2, and M4 for the neutron diffraction measurements (Figure 1c). For the study reported here the "wet" pretested samples M2 and M4 represent coupled chemomechanical altered states, the "dry" M5, a mechanically superimposed residual strain state. The loading path and duration of the three samples varied. These time- and stress-dependent effects cannot be resolved with the applied method. With the neutron diffraction, we determine the vertical extent of the damage zone and the associated grain-scale deformations. Next to the pretested samples a reference sample, M0 was cored from an untested Carrara marble beam, to assess the initial, inherited residual strain state.

2.3. Neutron Diffraction

Neutron diffraction is the application of elastic neutron scattering to determine the atomic structure of a material. The advantage of neutrons, compared to X-ray diffraction is their penetration depth of up to tens of centimeters (Holden et al., 1995). This allows evaluating the internal structures of polycrystalline materials without surface or edge effects. Diffraction measurements utilize the reflective properties of atoms ordered in crystal lattice planes, following Bragg conditions (Bragg, 1924). These structures show specific reflection angles (2θ°) and specific peak positions (d_{hkil}) in the according diffraction patterns (Figure 2a). Measurements of residual strains rely on the elastic deformation within polycrystalline materials, which cause changes in the spacing of the lattice planes (d-spacing) relative to their strain-free conditions. These distortions of the lattice planes alter the reflection angle and with it the peak position in reference to a strain-free or undistorted lattice (d_{0hkil}) (Noyan & Cohen, 1987; Withers & Bhadeshia, 2001b). A shift in the peak position is thus a measure of the elastic microstrain ε_{hkil}, estimated by

$$\varepsilon_{hkil} = \frac{(d_{hkil} - d_{0hkil})}{d_{0hkil}} \quad (1)$$

Where a positive peak position deviation indicates extensional strain, a negative value is a relative contraction (Figure 2b). These types of microstrains are also termed intergranular strains as they have been linked to elastic strains locked in between grains or crystals (Withers & Bhadeshia, 2001a). Distortions of lattice planes can also alter the dispersion of the reflected neutrons resulting in changes of the peak positions and shape metrics (Ungár, 1998). Our neutron diffraction measurements were conducted at the SALSA strain diffractometer at the Institute Laue-Langevin (ILL), Grenoble, France (Figure 2c) which is specified to measure the peak positions in 2θ° space, with a precision of approximately $\pm 3.5 \times 10^{-5}$ Å (Pirling et al., 2006). Assessment of peak shape metrics like the full-width at half maximum (FWHM), which signifies plastic deformation within grains and crystallites, are therefore viewed as subsidiary and are reported in Supporting Information S1.

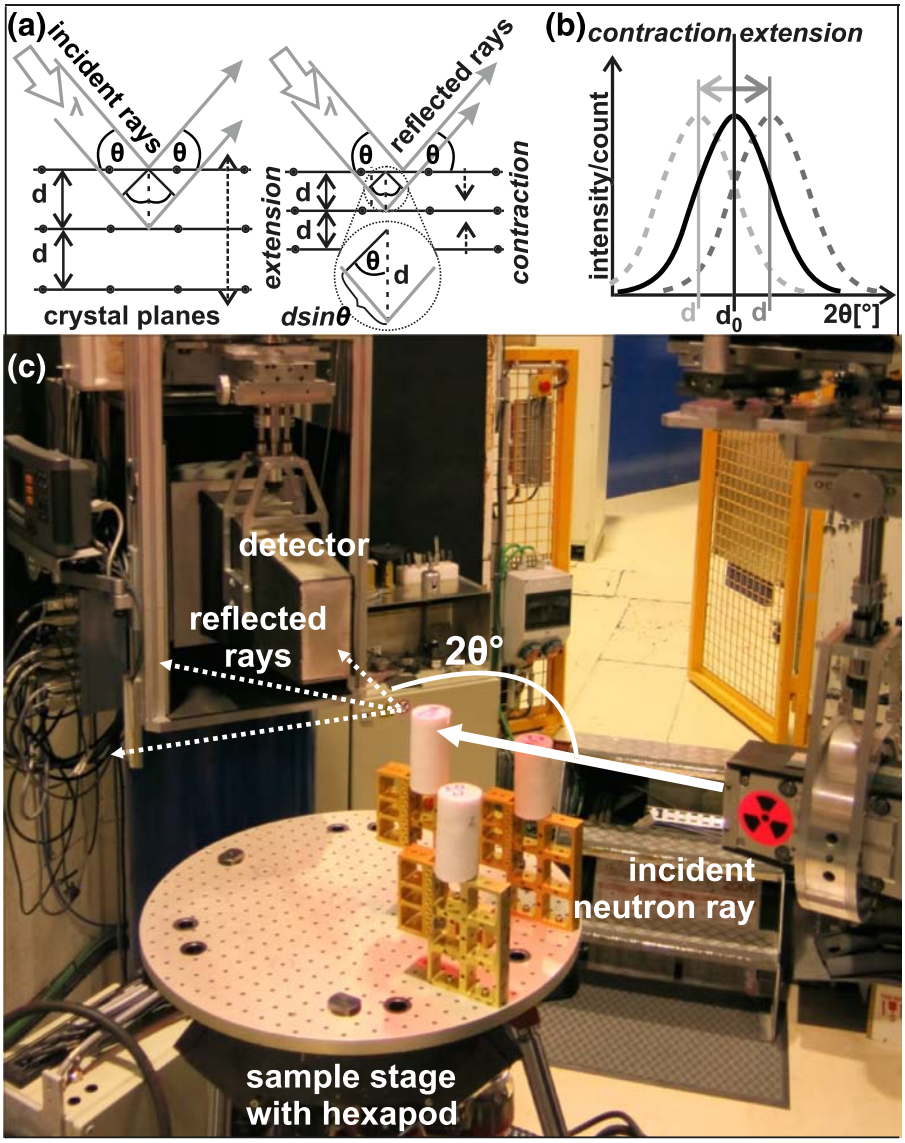

Figure 2. (a) Angle dependence of incident and reflected rays due to crystal lattice d-spacing and (b) schematics to evaluate intergranular elastic strains by peak position shift (c) SALSA diffractometer and experimental setup.

2.4. Measurement Protocol and Strain Estimation

SALSA measures small sections of diffraction pattern spectrum covering mainly single reflection peaks. For this study, neutron diffraction data were collected of diffraction peaks corresponding to crystallographic planes $\{1\bar{1}20\}$, orthogonal to the *a* axis, and {0006}, orthogonal to the *c* axis. By measuring these two orientations we can describe the unit cell of the calcite crystal. Additionally, $\{10\bar{1}4\}$, a prism face, was measured alongside with $\{1\bar{1}20\}$ due to the close position of the diffraction peaks in the recorded spectra. At SALSA, the thermal neutrons flux is continuous with an intensity of $\nmid 5 \times 10^7$ ns^{-1} cm^{-2}. We measured with a wavelength of $\lambda = 1.64$ Å. Neutron wavelengths are selected by a double-focusing monochromator, and SALSA is equipped with radial focusing collimators for a precise gauge volume, in our stud of 40 mm^3 ($2 \times 2 \times 10$ mm).

The geometry of the experimental setup, shown in Figure 2c, is chosen with the detector positioned in regard to the direction of the sample to measure with the scattering vector parallel to the pretesting

loading direction x (hereafter referred to as axial strain, ε_x), or perpendicular, in y (hereafter referred to as tangential strain, ε_y, Figure 1c). Samples are then manually adjusted and placed horizontally to collect data along the z axis from the notch or in the case of the reference sample M0 from its upper surface to the bottom of (hereafter referred to as vertical strain, ε_z). At each measurement point, strain was measured in the three spatial orthogonal directions (Figure 1c). Sampling progressed in 0.5 mm steps of gauge volume from the surface or notch for the first 5 mm below before the interval was increased to 10–20 mm for the rest of the samples M2, M4, and M5. Steps were again reduced to 0.5 mm for the 5 mm from the bottom of the sample in M0. Results provided at least 25 measurement points per sample, direction, and crystal lattice planes. Each measurement point comprises 4,000 scatter counts.

Diffraction data were fitted using a single Gaussian peak fit in LAMP (Large Array Manipulation Program), the standard diffraction fitting software provided by the ILL (Richard et al., 1996). An individual background fit clearing standard instrumental errors has been applied to all diffraction spectra. In addition to the acquisition of the peak position of the three crystal planes, we estimated the unit cell volume regular calcite crystal structure, based on $\{1\bar{1}20\}$ and {0006} measurements. Strain-free reference states (d_{0hkil}) are theoretically derived based on calcite single crystal unit cell dimensions (Rao et al., 1968). To isolate the effects of the mechanical and chemomechanical pretesting (see section 2.2), these calculations were compared to the untested sample M0. Serving as a reference state, the mean peak position along the measured section of M0 was used exempt the five measurement points near the surface top and bottom, as they might show edge effects.

3. Results

3.1. Residual Strain State of Carrara Marble

Neutron diffraction data of the pristine sample M0 showed an overall contractional residual strain state throughout the vertical measured section and sample spatial orientations (x, y, and z, Figures 3 and S2). The sum of the unit cell volumetric lattice strain in the three spatial directions was nonzero (Figures 3 and S3). The magnitudes of residual strains varied by measured crystal planes, ranging from an average of −435 (±455) μstrain in $\{10\bar{1}4\}$, to −890 (±500) μstrain in {0006}, to −2015 (±697) μstrain in $\{1\bar{1}20\}$ in all sampled spatial orientations (Figure 3). The unit cell volumetric strain related to an average volumetric contractional state of about −370 (±160) μstrain (Figure 3). We use this initial strain state as the background against which the changes in the pretested samples, described below, are interpreted.

3.2. Strain State Pretested Carrara Marble

Here we present the principal observations of the residual strain state measured in the pretested samples working downward from the notch tips to the base of the samples (Figure 1c). The overall residual strain states of the preceded tested samples M2, M4, and M5 were contractional (Figures 4–6). Extensional, intergranular axial strains, in reference to the mean strain state of untested sample M0, were observed in all samples in the measurement points 10–20 mm (in z) below the notch. Beyond these points, the strain states were contractional and approached the reference mean strain of M0 toward the neutral axis. Measurements below the neutral axis of the samples exhibited a less contractional strain state than the reference strain state. The crystallographic planes {0006} and $\{10\bar{1}4\}$ showed a greater absolute deviation from the reference sample M0 (up to 4,000 and 2,000 μstrain, respectively), while crystal planes of $\{1\bar{1}20\}$, kept a compressive strain of about −2,000 μstrain in all samples and all spatial directions (Figures 4–6). A general difference between the dry (M5, Figure 4) and the wet pretested (M2 and M4) samples was observed in the vertical extent and magnitude of the induced strain pattern (Figures 5 and 6).

3.2.1. Strain State in the "Dry" Mechanically Pretested Case

The overall residual strain state of the mechanically dry pretested sample M5 was contractional for all three crystal planes and in the unit cell volumetric strain (Figure 4). However, the strain state within the first 5 mm below the notch (in z) of the sample was extensional, markedly in the axial direction (Figure 4a). The magnitude of these induced extensional intergranular axial strains just below the notch-tip range from ~500 to 1,800 μstrain in $\{10\bar{1}4\}$ (Figure 4a), ~1,000 to 3,500 μstrain in {0006} (Figure 4b), and ~200 to 400 μstrain in unit cell volumetric strain (Figure 4d). In opposition to the extensional axial strain state, tangential strains

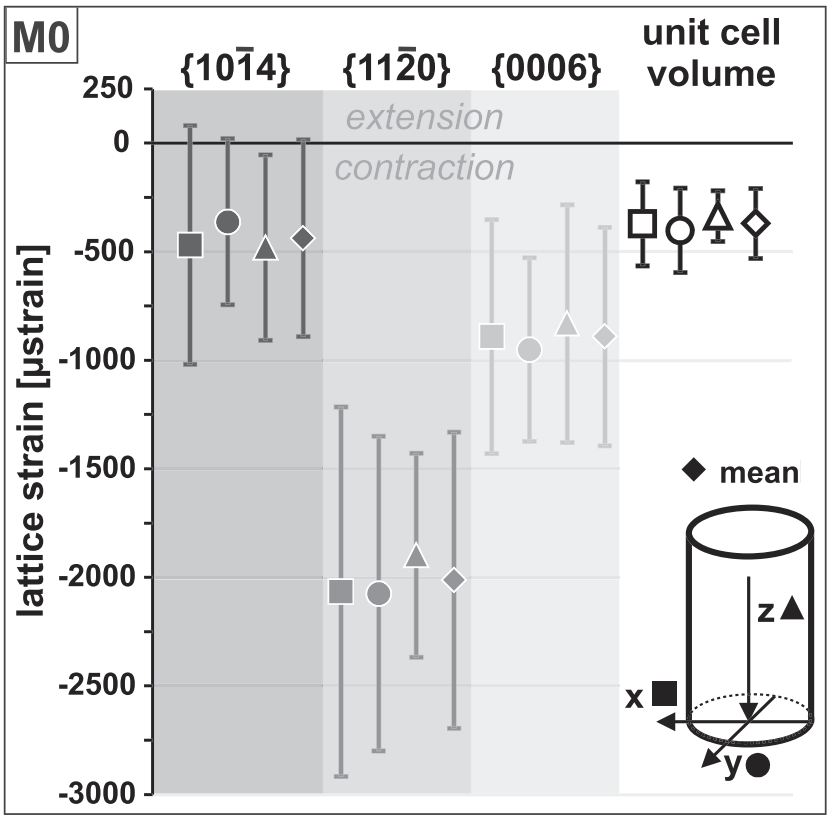

Figure 3. Average residual lattice strains of sample M0 in the three spatial direction and their mean in crystal planes {10$\bar{1}$4}, {11$\bar{2}$0}, {0006}, and the unit cell volume. The overall strain state is contractional. Magnitudes vary by crystal planes and less by spatial orientation.

were contractional, in the range of about −250 to −500 µstrain in {10$\bar{1}$4}, −2,500 to −3,500 µstrain in {0006}, and −500 to −600 µstrain in the unit cell volume below the notch.

3.2.2. Strain State in the "Wet" Chemomechanically Pretested Cases

In the wet pretested samples, a change in the assessed crystal lattice planes and the unit cell volume in reference to M0 was detected up to 30 mm below the surface along the vertical measured section (in *z*, Figures 5 and 6). The unit cell volumetric strains were in an overall contractional state between −1,000 and −50 µstrain in all spatial directions, while the individually measured crystal planes exhibited local extensional strain primarily in the *x* direction (Figures 5 and 6).

In the axial direction of sample M2 an absolute extensional strain state was observed within the first 2 mm below the notch in crystal lattice planes {0006} (Figure 5b). In crystal planes {11$\bar{2}$0}, the strain deviated from the reference sample M0 of up to 1,000 µstrain (Figure 5c). In the unit cell volume, the axial strain corresponds with the reference strain state up to ~12 mm below the sample surface (Figure 5d). Below these first millimeters, up to 25–30 mm of the vertical section, the strain state in the axial direction showed a strong contractional strain state in all measured crystal lattice planes. These strong contractional axial strains were contrasted by less contractional strains (in reference to M0) in the *y* and *z* directions.

Sample M4 showed extensional axial strain at the notch tip of ~900 µstrain, as well as at 17 mm of ~1,400 µstrain in lattice planes {10$\bar{1}$4} (Figure 6a). In between these extensional strains, a steady increase and a subsequent decrease in contraction was observed which terminates at ~16 mm. Extensional strain states at 15–20 mm (in *z*) were also observed in diffraction peaks of crystal planes {0006} of ~500 to 1,800 µstrain (Figure 6b) and less contractional strain in the unit cell volume (Figure 6d). The superimposed change in reference to the state of M0, vertically exceeds the visible fracture tip (Figure 1f) by about 1.5 mm, below this, the strain state in all spatial directions is contractional.

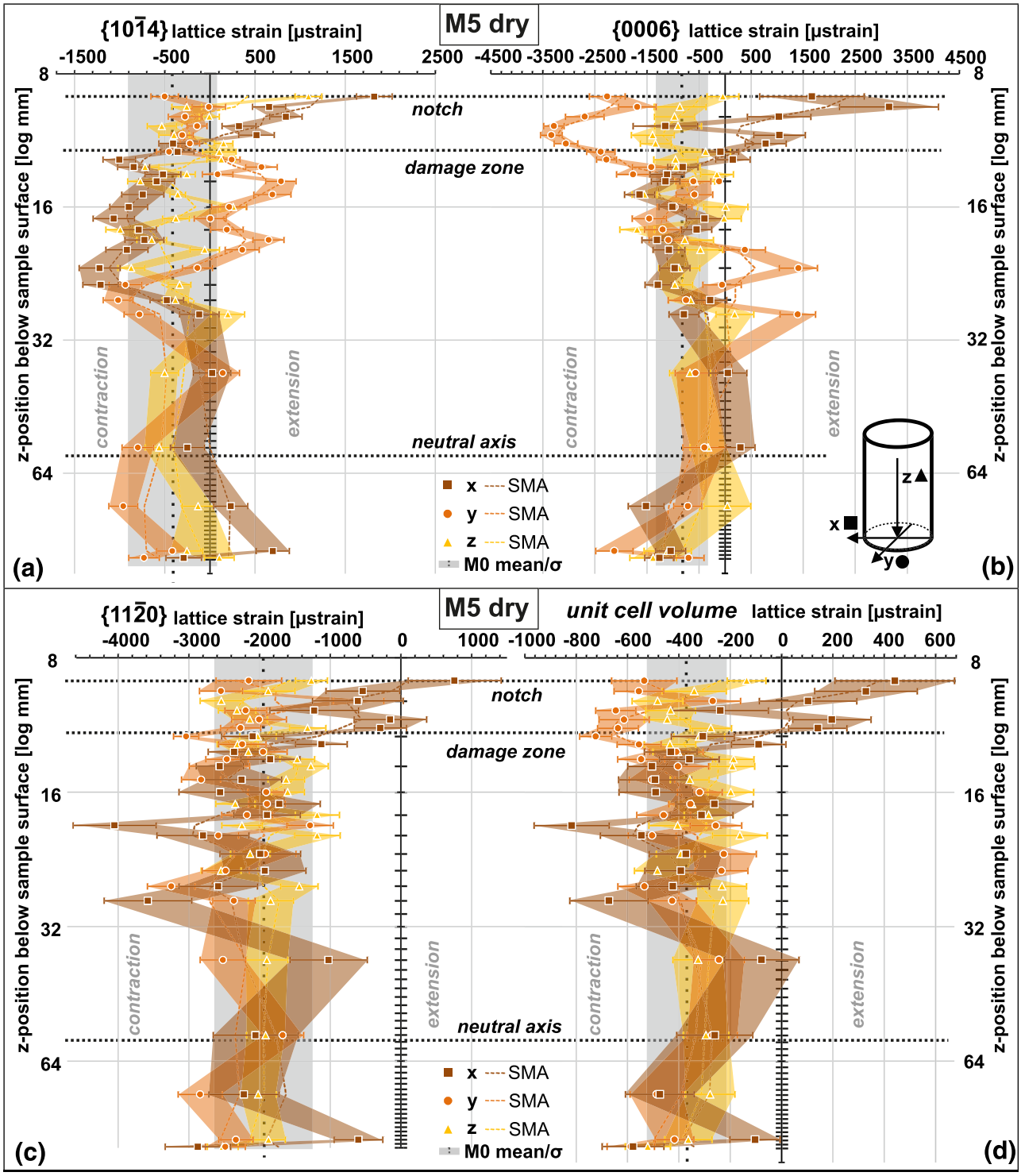

Figure 4. Residual lattice strain of single crystal plane and unit cell volume of sample M5 along the vertical measured section. (a) Crystallographic planes {10$\bar{1}$4}, (b) {0006}, (c) {11$\bar{2}$0}, and (d) the unit cell volume. The spatial directions are indicated by color and symbol. Strains are given with their error bounds and a three-point running average in dashed lines (SMA). Vertical black dashed line represents the mean, the gray bound the standard deviation of reference M0. Vertical extent (in z) of the notch is inferred from a thin section image (Figure 1d, Voigtländer et al., 2018). The extent of the damage zone is discussed in the text.

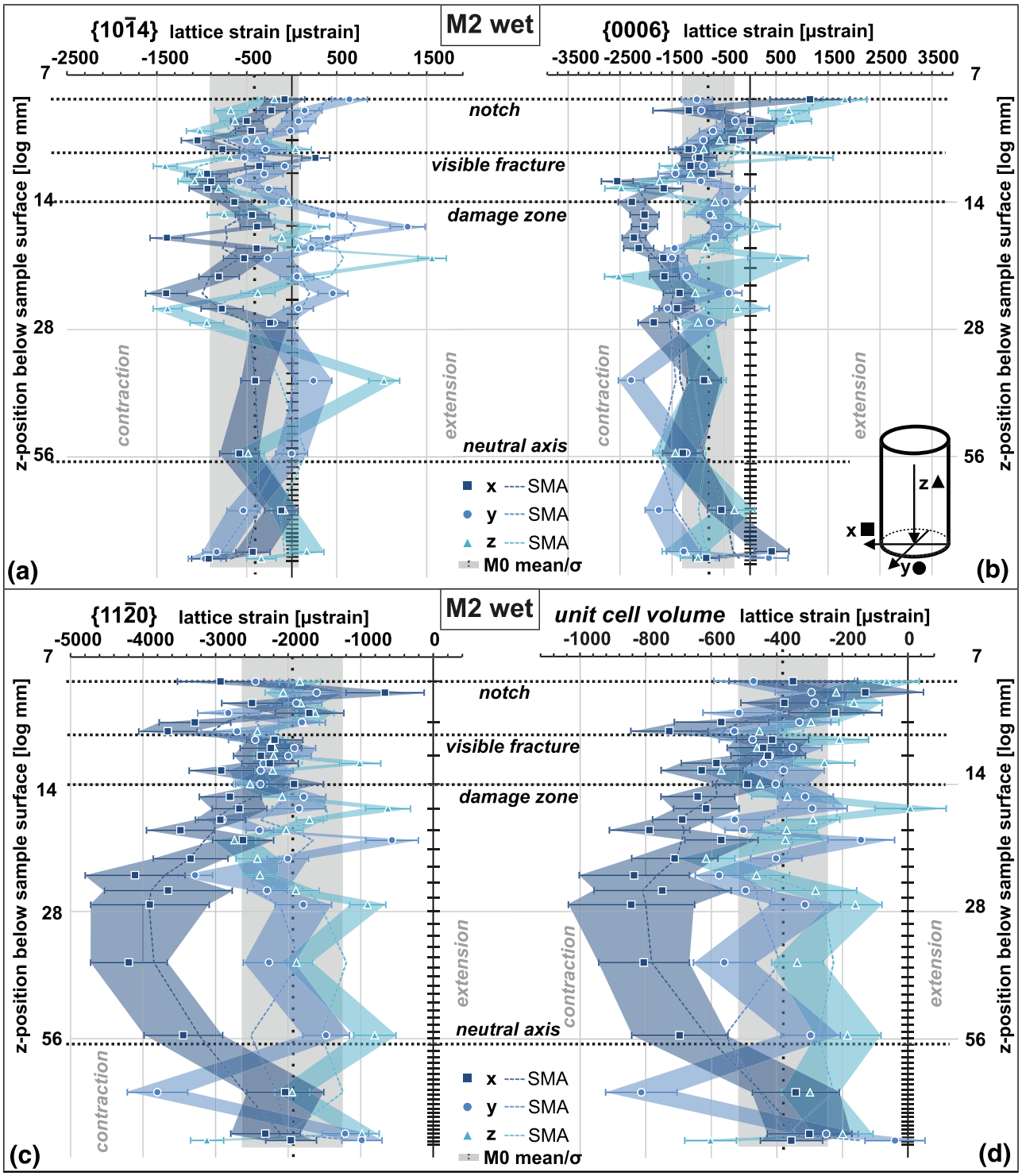

Figure 5. Residual lattice strain of single crystal plane and unit cell volume of sample M2 along the vertical measured section. (a) Crystallographic planes{10$\bar{1}$4}, (b) {0006}, (c) {11$\bar{2}$0}, and (d) the unit cell volume. The spatial directions are indicated by color and symbol. Strains are given with their error bounds and a three-point running average in dashed lines (SMA). Vertical black dashed line represents the mean, gray bound the standard deviation of the reference M0. Vertical extent (in z) of the notch and visible fracture are inferred from a thin section image (Figure 1e, Voigtländer et al., 2018). The extent of the damage zone is discussed in the text.

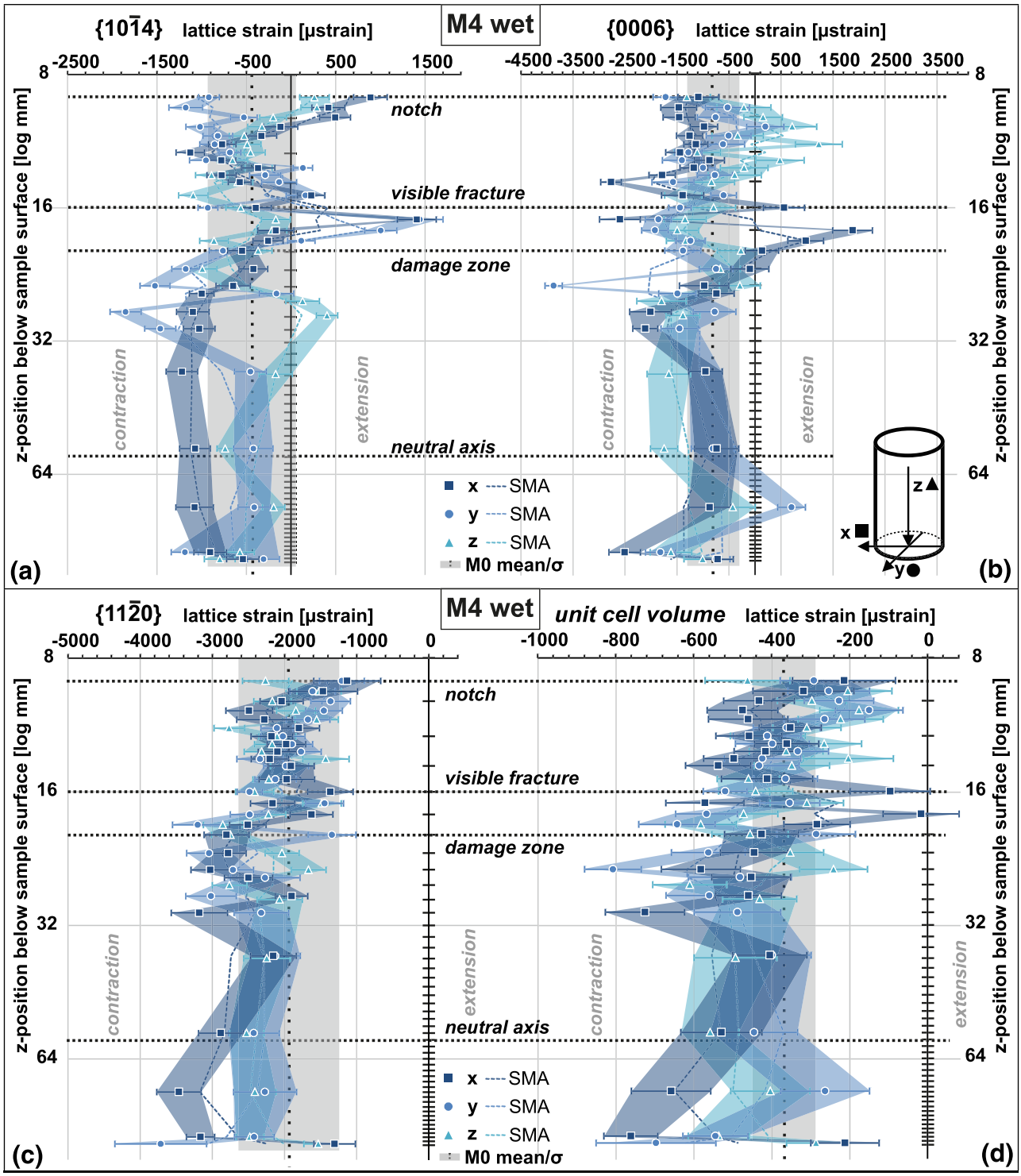

Figure 6. Residual lattice strain of single crystal plane and unit cell volume of sample M4 along the vertical measured section. (a) Crystallographic planes {10$\bar{1}$4}, (b) {0006}, (c) {11$\bar{2}$0}, and (d) the unit cell volume. The spatial directions are indicated by color and symbol. Strains are given with their error bounds and a three-point running average in dashed lines (SMA). Vertical black dashed line represents the mean, gray bound the standard deviation of the reference M0. Vertical extent (in z) of the notch and visible fracture are inferred from a thin section image (Figure 1f, Voigtländer et al., 2018). The extent of the damage zone is discussed in the text.

4. Discussion

We measured the residual strain of Carrara marble samples by neutron diffraction to better understand their influence on the rheology and how they are altered by time-dependent and environmentally enhanced deformation. Neutron diffraction techniques essentially measure the lattice planes of the crystallites. Due to the nearly randomized CPO of our Carrara marble (Figure S1) no distinct influence of texture on the diffraction pattern was expected. The peak position of the three measured lattice planes, $\{10\bar{1}4\}$, {0006}, and $\{1\bar{1}20\}$ in reference to strain-free positions represent/indicates the bulk intergranular strain state of the assessed gauge volume. In our experiment, it was ~2 × 2 × 10 mm (~40 mm^3), equivalent to ~20 grains. The measured magnitude and sign represent the sum of all residual strains of the individual crystallographic planes within that gauge volume. The strain state is discussed concerning this representative elementary volume (REV) of rock.

First, we discuss the initial residual strain state of Carrara marble with the observations of the untested reference sample M0. Second, we compare the residual strain of pretested samples, M2, M4, and M5 with the initial residual strain state of M0, to infer the role of the internal and external factors on progressive rock failure. We focus on how subcritical crack growth during the pretest have caused inducement and relaxation of initial residual strain state and speculate how the initial residual state might have influenced the progression and extent of damage during the pretest.

4.1. Initial Residual Strain State

The general expectation of the internal strain state of the untested sample M0 would be that, as there was no traction on the surface, the sample would be macroscopically in elastic equilibrium. Neutron diffraction data of the intact reference sample M0 showed, that the Carrara marble maintained contractional strains in the order of $\times 10^{-4}$ in the unit cell volumetric and $\times 10^{-3}$ in single crystal lattice orientations at the location and scale of the representative elementary volume (Figures 3 and S2). The sum of the unit cell strains in the three spatial directions was contractional by about −1,000 μstrain (Figure S3). If the sum is not equilibrated at this scale, it implies that the material has undergone deformation along and in-between grains (Pintschovius, 1992). Analogous experiments have shown that extensional and contractional strains are both present, in close proximity to each other on the local grain-boundary scale (Friedman, 1972; Gallagher et al., 1974; Holzhausen & Johnson, 1979). The bulk contractional residual strain state of our sample thus indicates that contractional strains dominate within the crystal structures measured in the diffraction gauge volumes along the vertical sample section. For our Carrara marble, we assume that the material deformed as a continuum with locking-in residual strains homogenously throughout the material while it was deformed and exhumed in the crust. Here, the sum of the measured gauge volumes is the representative elementary volume discussed in the following. In this context, we observed for our intact sample spatially isotropic unit cell volume strain magnitudes of −400 (±190) μstrain in x direction, −370 (±190) μstrain in y direction, and −340 (±115) μstrain in the z direction (Figure 3). We discuss the generality of these states and their implications for the interpretation of stress memory and first-order, highly idealized material properties in a stress-based framework. In detail, this assumption is not valid as a polycrystalline material like Carrara marble will have deformed and build up strain in a noncontinuous fashion across grain boundaries and crystals. However, this distinction is not resolved in our neutron diffraction measurements.

In geological studies, most residual strain data of rocks is considered as strain memory and interpreted regarding the potential paleo-stress field (Engelder & Sbar, 1977; Sekine & Hayashi, 2009; Zang & Berckhemer, 1989). A scenario of how the residual strains are locked-in, the Carrara marble would either be by the external tectonic forcing or internally organized by material properties during the formation of the Apuan Alps. For Carrara marble, it has been reported that the rocks were buried to a depth of 20 to 40 km when reaching metamorphic peak conditions (D1), followed by successive rapid exhumation up to a depth of 10–15 km (D2) (Balestrieri et al., 2011; Carmignani & Kligfield, 1990). Our samples showed a relative homogeneous microstructure and a near-random CPO (Voigtländer et al., 2018). These microstructures are the result of static recrystallization during these deformation phases (Molli et al., 2018; Molli & Heilbronner, 1999). Deviatoric stresses, which might have been arising from decompression and cooling during exhumation would have balanced each other when rock reached the surface (Zang & Stephansson, 2010). However, our data show, that residual strains still exist in the intact Carrara marble sample, M0. This would indicate that the residuals strains were induced, highly simplified speaking, under hydrostatic condition. The

potential to develop residual strains under hydrostatic conditions has been described by Savage (1978) for granites. Due to varying thermal expansion coefficients in the two considered materials by him, residual strains form due to the cooling rock bodies. Resulting shear stress at the interfaces of the two materials would lock-in elastic strains without volume or shape changes, similar to variational principles of Hashin and Shtrikman (Avseth et al., 2010; Hashin & Shtrikman, 1962; Watt & Peselnick, 1980). In a monomineralic material as the Carrara marble, this can be explained by considering the specific thermal properties of calcite. Calcite crystals show highly anisotropic thermal expansion coefficients, with expansion parallel to the crystallographic *c* axis and contraction parallel to the crystallographic *a* axis (e.g., Rao et al., 1968). In our Carrara marble, where we have randomly distributed orientations of the crystal axis, the highly anisotropic cooling response of the crystallographic axis of the calcite minerals would result in elastic mismatch and deviatory strains especially along grain boundaries with different crystallite orientations and thermal expansion coefficient. The calcite rock volume, would thus internally tense up during the general cooling. This thermally driven locking mechanism of strains, analogous to the tempering of glass, would probably affect the rheological properties of the rock and especially its strength (Bruner, 1984; Hoskins & Russell, 1981; Nichols & Abel, 1975).

In material science, the residual strain state is often interpreted concerning its effect on rheology and material strength (Toribio, 1998; Withers, 2007). Applying this broadly to rock, the inherited measured general contractional strain state of our Carrara marble can be described as a degree of rock strength. Rock strength is typically indicated in a stress-based framework. A first-order estimate, following Hooke's law, assuming a Young's modulus of 49 GPa (Alber & Hauptfleisch, 1999), and taking our measured mean unit cell volumetric strain of −370 μstrain of sample M0, equates to residual stresses of −18.1 MPa. To exploit residual strain measurements in a stress-based framework, elastic constants would need to be measured in the same material as well. In addition, if the estimated general residual stress state is compressive, like in our Carrara marble sample M0, this would exert indirect tensile stresses at the same time. The magnitude of the indirect tensile stress would be the contractional residual stress times the Poisson's ratio. Assuming a Poisson's ratio of about 0.19–0.29 (Alber & Hauptfleisch, 1999) the general residual stress state of our Carrara marble would indirectly stress the bulk material, in a first approximation, by about 3.4–5.2 MPa. Independent Brazilian indirect tensile strength tests of the same Carrara marble yield a bulk strength of about 5 MPa (Voigtländer et al., 2017). Accordingly, we interpret that the rock is near critically prestressed. Additionally induced contractional strains in the order of −400 μstrain though, could facilitate indirect tensile microcracks. The relaxation of residual strains is readily accomplished by microcracking, mainly along grain boundaries. The contractive prestressed or prestrained microstructure thus would define the fracture toughness and long-term fundamental strength of the rock. Residual strains would, at least partially, define the magnitude of external loading or stress intensity required to initiate or progress fracturing in intact rock. This is discussed in regard to the pretested samples in the following section 4.2.

Despite the uniform residual strain pattern in all spatial orientations along the measured section, we observed a distinct variation in the magnitudes of residual strains among the three measured crystal lattice planes, from an average of −435 μstrain in $\{1\bar{0}14\}$, to −890 μstrain in {0006}, to −2,015 μstrain in $\{1\bar{1}20\}$ (Figure 2). The variation of the magnitude of residual strain in the measured crystal lattice planes can be attributed to the crystal structure of calcite, which forms the Carrara marble. In crystallographic deformation experiments, the basal plane *c*, thus on {0006} $<1\bar{1}20>$, and especially the prism face $<r>$, on $\{1\bar{0}14\}$ $<2\bar{0}\bar{2}1>$, have been determined as common slip planes in calcite crystals (Barber et al., 2007; De Bresser & Spiers, 1997). While slip along $\{1\bar{0}14\}$ $<2\bar{0}\bar{2}1>$ is even active at room temperature and low critical-resolved shear stress (De Bresser & Spiers, 1997), *c* slip has only been found at high temperatures (Barber et al., 2007; Borg & Handin, 1967). Active slip on these planes would counteract the induction and locking-in of strain. Therefore, it can be argued that either during the formation of the Carrara marble less strain energy could be locked-in on crystal planes {0006} and $\{1\bar{0}14\}$ or that time-dependent relaxation since the Apennine orogeny took place preferentially on those planes. In crystal planes $\{1\bar{1}20\}$, on the contrary, higher magnitudes of residual strains can build up because they do not slip, but are in the *c* slip direction and thus elastic strains can preferentially be locked-in along those. The initial lower magnitude of compressive residual strains makes those crystal planes more susceptible to external forces and conditions and evoke a rheological anisotropy.

4.2. Superposition of Residual Strain State by Mechanical and Chemomechanical Pretests

During the inverted single-edge notch bending creep pretest samples M2, M4, and M5 exhibited various degrees of macroscopic strain at the notch tip and exhibited a remnant strain upon unloading (Voigtländer et al., 2018). Thin sections of notch area showed single localized fractures initiated at the notch in the samples, M2 and M4 tested with water present at the notch during the pretest (Figures 1e and 1f). The effect of this induced damage, its extent, and the possible mechanisms involved on the residual strain state we assess by comparing the measured residual strain states against the intact initial residual strain state of sample M0. Knowing the initial residual strain state of our Carrara marble (Figure 3) we can then speculate how this might have influenced the progression and extent of damage during the pretest. By this, we ultimately, want to infer the relative role, and control, of internal and external factors on progressive rock failure. Slight initial variations samples may have implications on the degree of inferred induced and relaxed residual strains in the pretested samples.

The overall pattern of alteration of the residual strain state by pretesting the samples corresponded to the loading configuration (Figures 1a and 1b), as expected. In all three samples, spatially heterogeneous superposition of the initial residual strain state was visible along the vertical axis. The rebound pattern follows the graded externally applied stress, the principal stress directions, and stress concentrations due to the inverted single-edge notch three-point bending configuration (Figure 1a and 1b). We define the vertical extent of the superposition of residual strains as the "damage zone" (Figures 4–6). The vertical extent of the induced strain pattern differs remarkably from the environmental conditions during pretesting. The strongest superposition of the initial residual strain state is observed along $\{10\bar{1}4\}$ lattice planes, the least along $\{1\bar{1}20\}$. The magnitude of induction of residual strains corresponds to the variation in the initial magnitude of each measured crystal lattice planes in the reference M0. Even though the residual strain state is altered by the external factors, the overall residual strain states of pretested samples are still in contraction (Figures 4–6).

Spatially variable changes in residual strains of the pretested samples exhibited two levels of internal self-constraint, as individual crystallites are unable to expand or contract as they would like in response to any external loading because of the concomitant expansion and contraction of their neighboring crystallites. One level is due to the bonded polycrystalline bulk structure of the sample and another due to the interdependency of the calcite crystal axis. The first level we discuss with the focus on crystal lattice planes $\{10\bar{1}4\}$, along which we observed the strongest superposition in the samples spatial orientations. Comparing all three measured spatial orientations, extensional strains in the x direction near the notch or fracture tip are countered by contractional strains in the y and z directions (Figures 4a, 5a, and 6a). Because our neutron diffraction measurements were conducted on unloaded samples, the relationship does not follow the Poisson's ratio as would be expected during loading conditions. Due to the unloading, elastic strains could rebound at the termination of the pretest where they were not obstructed by any permanent damage around them in the vertical section. Due to tensile stress concentration near the notches, induced and relaxed strains showed the strongest deviation in comparison to reference sample M0 in the major principal deviatoric stresses in the axial direction of the pretest configuration. This may explain the local extensional strain enhancement near the notch tip in M5, as well as the stronger contractional strain below until the neutral axis (Figure 4a). The stronger contraction, compared to the mean reference state, would be the effect of the induced extensional strains in the section above, which instead of rebounding the elastic strain back to the initial state created a strain shadow or deficit below the permanent deformation. Holzhausen and Johnson (1979) showed this pattern and response conceptually in analogous experiments of bent beams. In the three-dimensional case, the rebound or relaxation of the strain pattern might be less pronounced as a reduction in one spatial direction can be balanced by an increase in one or another.

The second level of accommodation of the strain change is observed within the crystals structure, as single axis is not able to rebound freely. This is the type of internal self-constraint within the crystal axis as has been described regarding thermal stressing (Meredith et al., 2001). An internal self-constraint is obvious in comparison of the crystallographic planes $\{0006\}$ and $\{1\bar{1}20\}$ and the corresponding changes in the unit cell volume. Because unit cell volume has been calculated from the $\{0006\}$ and $\{1\bar{1}20\}$ measurements, corresponding changes of the a and c axes are subsumed within. Within the damage zone of samples M2 and M4, the unit cell volumetric strain in all spatial directions is close to the initial reference mean strain state of M0 (Figures 5d and 6d). Inducement or relaxation of strain along one axis was likely balanced by the

other. Below the damage zone, the unit cell volume strain diverges more, especially in the axial strain. Within this section, the dominant crystal lattice plane for the strain state is {1$\bar{1}$20}. Along these lattice planes, strains could have been built up during the pretesting, as glides and slides, which might relax strain, are countered by the initially high contractional residual strain magnitudes (Figure 3), resulting in a local strain enhancement.

The spatial variable introduction and relaxation of residual strains during the pretesting produced a spatial anisotropy within the initially spatially isotropic residual strain state in Carrara marble (Figures 3–6). It has been observed that spatial persistence of residual strains would be aligned with preferred orientations of fractures in rocks (Friedman & Logan, 1970; Weinberger et al., 2010; Zang & Berckhemer, 1989). If the residual strain is spatially inhomogeneous, it is expected that the local strain may lead to a change in direction of fracture propagation that is not necessarily aligned with the global stress direction (Friedman & Logan, 1970; Lee et al., 2011). It has been shown for engineering materials, that the propagation of a single fracture is influenced by the residual strain state at its tip (Withers, 2015). If the residual strain state at the fracture or notch tip is contractive, it poses a counterforce against applied tensile stresses and thus retards further fracture propagation. Contrary, in an extensional residually strained state, fracture propagation is likely to be enhanced (Withers, 2015). If we take into consideration the initial overall compressive residual strains within the representative element volume and the sum of them found in the Carrara marble (Figure 3), they should have counteracted the induced extensional strain during the pretesting. The unloaded state we have measured though shows extensional strain in the dry, and less contractional strains in the wet pretested samples. Reloading this "new" preexisting strain state would face less resistance to critical deformation and macroscopic failure, thus the progressive damage state. Implying that these strain or stress components are additive, then rocks can potentially fail under significantly lower external loads than expected. It has been shown that hygroscopic or thermally triggered expansion adds to preexisting extensional strains by mechanical loading (Collins & Stock, 2016; Voigtländer et al., 2018).

The environmental conditions during the pretest seem to have largely affected the mechanisms and pattern of relaxation and induction of strains, and thus the progressive damage state. While the vertical extent of superposition of the initial strain state is greatest in wet samples M2 and M4 (Figures 5 and 6), the magnitude of induced extensional strain is highest in the dry sample (Figure 4). Mechanistic explanations for the introduction and relaxation of residual strains in rocks are still preliminary (Scheffzük et al., 2004; Varnes & Lee, 1972). The inducement of extensional strains and relaxation of contractional residual strains are probably complementary and conditioning processes. Similar to the rate and magnitude of subcritical damage mechanisms, knowledge on the induction or release of residual strain energy over time is still limited (Chen et al., 2015; Engelder, 1993; Nichols, 1975). In the following, we discuss possible mechanisms regarding the influence of the "dry" and "wet" pretest conditions that (i) build up strain or (ii) lead to relaxation, in both cases contributing to the progressive damage.

4.2.1. Superposition by Subcritical Mechanical Stress in "Dry" Condition

In the "dry" pretested sample M5 the strain state is particularly altered at the notch and in the axial direction where tensile stress had been greatest and the geometry fostered stress concentration. The stress was not critical to initiate a macroscopic fracture, as only some grain boundary decohesion around the notch was evident in thin section analysis (Figure 1d, Voigtländer et al., 2018). From the microstructural analysis, we would assume that the sample was still intact and has the same fracture toughness as the untested sample. From the residual strain measurements though, we see differences in comparison to the reference sample M0. The residual strain magnitude is reduced and even in extension in the first 5 mm below the notch, in all three measured crystal planes and an expansion of the unit cell volume in the x direction (Figure 4). The measured gauge volumes in these millimeters below the notch we call the damage zone. We attribute these strain states to damage mechanisms which were incomplete in the creation of new surfaces. Even though inelastic intergranular deformations in calcite, like grain boundary sliding, can be activated at room temperature (Passchier & Trouw, 2005), it seems that the subcritical loading has not fully facilitated the necessary critical stress. Thus, they caused no or little relaxation and instead locked-in extensional strains (in x direction) by local, probably only partial but permanent plastic deformation like glides, tilts, and twists of grain boundaries (Platt & De Bresser, 2017). Even small induced deformations would lead to residual strain buildup due to the dense, brittle, and self-constraining microstructure of the Carrara marble. It has

also been shown by Darling et al. (2004) that even though deformations at the grain boundaries make up only a few percent of the material volume, they can dominate the average lattice strain of the REV.

The residual strain state along the vertical measured section in the dry sample M5 mimics the expected stress gradient and orientation dependency found in beam theory of material sciences (Holzhausen & Johnson, 1979; Timoshenko & Goodier, 1970). Below the damage zone, there is little to no superposition. At the bottom of the samples, where stress magnitudes were also high but due to the loading configuration in compression, the strain state is close to the mean reference state. This can be expected, as rocks and material bonds are generally stronger in compression than in tension (Damjanac & Fairhurst, 2010). Dry mechanisms to lock-in strain or to relax are controlled by the applied stress magnitude and mode. Brantut et al. (2014) showed that failure of rock, though in compression, occurs at the same amount of inelastic strain, independent of the loading rate. The induced residual strain, although disparate from the use of inelastic strain as a proxy in the aforementioned study, indicates that the amount of strain (energy) was not met to initiate a fracture and possibly fail, independent of the longer pretesting period of sample M5 (section 2.2). To initiate and progress a fracture in a simple Griffith crack scenario, either the applied stress would need to be risen or the conditions altered. The introduction of water can readily change the potential surface energy and shift the Griffith curve from a nonpropagating to a propagating crack (Lawn, 1993; Sadananda et al., 2017). This could be observed in dry Carrara marble samples loaded in the same testing configuration which would not fracture and fail at loads ≥80% of the fracture toughness, unless water was introduced (Voigtländer et al., 2018). This behavior has also been reported for other geomaterial and engineered materials (Malkin, 2012; Rehbinder & Shchukin, 1972).

4.2.2. Superposition by Subcritical Mechanical Stress in "Wet" Conditions

The "wet" pretested samples document the combined influence of subcritical loading conditions and reactive fluid on the residual strain state. In reference to the dry sample M5, the vertical extent of the damage zones is greater in the wet samples M2 and M4 (Figures 5 and 6). Within these sections the residual strains are extensional only in the measured crystallographic planes but not for the unit cell volumetric strain. Residual strains in the x direction are superimposed to a less contractional state in reference to M0. In microstructural thin section analysis of the notch area localized developing fractures were visible in both samples. The visible fracture tips were at a depth of ~12 mm in M2 and ~16 mm in M4 (Figures 1e and 1f). The fractures are localized and follow grain boundaries (Voigtländer et al., 2018). Regarding the mechanisms altering the residual strain state, the creation of traction free surfaces by a progressed fracture is assumed to be a key control (Friedman & Logan, 1970; Nichols & Abel, 1975). However, in our samples, the effect of the local relaxation of residual strains seems to be weaker on the bulk measurement than the introduction of strains, where a small fraction of grain boundaries affect the gauge volume (Darling et al., 2004). The general assumption that microcracks and fractures relax internal elastic strains by creating traction-free surfaces may only be confirmed (i) at the very local level and (ii) for cracks near free surfaces where they can result in volumetric extension. As the initiation or progression of a fracture entails the redistribution of the stresses that caused the process in the first place. However, the localized fracture is within bulk material where crystallographic planes are still in contraction. In the interior of the sample, the concomitant grains around the narrow fracture path dominate the residual strain state of the measured gauge volume. In the vicinity of the fracture tips, we observe more extensional strain states, similar to the notch area in the dry sample, indicating the introduction of elastic strains, without the creation of new surfaces. Another, not yet further investigated feedback could arise from fracture energetic perspective because residual strain stores energy which will likely affect the dynamics of brittle fracturing by providing additional fracture energy if released (Davies et al., 2012; Hill, 1963). As brittle intergranular damage can release stored strain energy, its dissipation contributes to further brittle fracture progression or the induction of strains ahead of the fracture (Lawn, 1993; Withers, 2015).

The combined effect of the mechanical loading and the wet conditions in samples M2 and M4 likely lead to the initiation of the fractures observed in the thin sections. During the pretesting, material bonds were mechanically strained in extension, which likely lowered the activation energy for chemical reactions, resulting in the rupture of the bonds and the progression of the fracture at loads ≥80% of the fracture toughness. This is in agreement with Griffith flaw extension theories (Lawn, 1993; Sadananda et al., 2017). Though the slightly higher deadweight loading in comparison to the dry pretested sample (80–85% compared to 77% K_{IC}) cannot completely be ruled out of having had an effect, chemomechanically enhanced subcritical crack

growth in our pretesting configuration would have caused a positive feedback on the stress intensity, at the same loads. Chemical and mechanical reasons for enhanced damage and strain changes in rocks in wet environments have traditionally been discussed separately. Stimulated by material sciences research, the interactive nature and positive feedback of chemical and mechanical mechanisms have recently raised increasing interest. Stress corrosion cracking has been introduced to geosciences and is assumed to be an important control in rock mechanics and Earth surface processes (Atkinson & Meredith, 1987; Brantut et al., 2013; Eppes & Keanini, 2017). Stress corrosion cracking is an umbrella term for mechanisms which involve lowering of the activation energy for chemical processes, by thermal or mechanical strain energy. In the case of calcareous Carrara marble, the chemical process would be dissolution. In rock mechanics application, the enhancement of this chemical process is generally considered to be due to externally applied stress. The effect of residual strains have been mentioned but not included in numerical models or interpretations of stress corrosion tests (Atkinson & Meredith, 1987; Potyondy, 2007). In material sciences, residual strains have been recognized to be integral parts of these chemically enhanced progressive fracture mechanisms, especially if the strain state is extensional (Toribio, 1998; Withers, 2007). General enhancement of dissolution kinetics due to strain or stress concentration has been experimentally demonstrated in calcite crystals (Schott et al., 1989). Based on the initial contractional residual strain state we would expect that they delayed stress corrosion mechanisms in our "wet" pretested samples M2 and M4 until induced extensional strains outpaced the residual strains and lowered the reactivity limit. Residual intergranular strains, their magnitude, and sign as well as their variation in the measured crystallographic planes, could mechanistically explain observed general effects of stresses on chemical kinetics and the anisotropy of crystal reactivity, in dissolution and weathering (Pollet-Villard et al., 2016; Wheeler, 2018).

Besides chemical effects, there seems to be a mechanical effect of water on the superposition of residual strains. The wetting of weakly interlocking grain boundaries can lower the resistance to friction, by lubrication and wedging (Baud et al., 2000; Nicolas et al., 2016). While dry slides would be built up strains by friction and wear, wet, lubricated, smooth interfaces can glide along each other without the inducement of new strains (Homola et al., 1989; Violay et al., 2014). This can explain the remaining overall, and average contractional unit cell volumetric strain state of the wet samples (Figures 5d and 6d), although samples M2 and M4 exhibited greater vertical damage extent than dry sample M5. Likewise, the lower overall extensional residual strains observed in wet samples may derive from more efficient relaxation after the pretests, as grain boundaries slides could be reversed. While we observed chemomechanical enhancement of subcritical crack growth, the presence of water also mitigates strain built up or the locking-in of extensional strains. This effect has not been described before but may play an important role especially in progressive rock failures in the upper crust, where water is ubiquitously present.

5. Conclusions

We addressed the impact of residual strains on progressive rock failure, a subject of considerable field, experimental, and numerical studies. The importance of internal controls on progressive rock failure has been stressed in hazardous rock slope failures, but concepts and proxies to assess them have not yet been clear (Bjerrum & Jørstad, 1968; Krautblatter & Moore, 2014). Progressive rock failure studies in the context of building materials such as Carrara marble façade panels have highlighted material properties and the internal state (Koch & Siegesmund, 2004; Siegesmund, Ruedrich, et al., 2008). They showed how the extent of progressive damage is controlled by environmental conditions. It could be shown that the bowing potential of these panels can be linked to material properties including residual strains (Scheffzük et al., 2004). Our study differs from previous work on progressive rock failure in that it considers internal controls and the change thereof in a systematic and conceptual framework. We assessed the internal state with the proxy of residual strain states, measured with neutron diffraction techniques. The results from our study provide first insights into the residual strain state of Carrara marble and the superposition by mechanical and chemomechanical alteration in relation to what is commonly referred to as the stress memory.

We further documented the relationship between the initial state and the response of the rock to external loading. Results also show how dry or wet pretesting conditions affect the damage mechanism and the resulting transient residual strain state. Our experiment demonstrates that subcritical mechanical and chemomechanical external loading can relax stored contractional residual strains and induce extensional

strains in Carrara marble samples. We, therefore, hypothesize, that the initial residual strain state defines the general efficiency of external drivers to progressively weaken the rock. Our results show that the overall residual strain state of our Carrara marble is contractional, and thus provides an initial counterforce toward extensional stresses. The homogeneous and isotropic initial state of the rock is readily superimposed and a spatial anisotropy in the strains introduced. Varying magnitudes of residual strain along the measured crystal lattice planes also indicate a microstructural anisotropy, which is likely exploited by external conditions and loading.

We could show how, in principle, internal states can be investigated. For the study of progressive rock failure, this implies that both time dependency as well as internal state dependency need to be considered and at best be quantified. Quantification of the residual strain states of rocks thus helps to explore a wide range of challenges and characterize mechanical and rheological properties of rocks. Residual strain states could also be used to define the initial material strength, independent of an applied stress, and extensional strains could be used to describe internal damage states. Neutron diffraction methods, therefore, contribute to better characterize the internal state of rocks and anticipate progressive rock failures.

Data Availability Statement

Supporting information S1 can be obtained from the journals homepage and contains additional Figures S1, S2, and S3. Data can be accessed via this site (http://doi.ill.fr/10.5291/ILL-DATA.1-02-149).

Acknowledgments

Diffraction measurements were made possible by a granted proposal (1-02-149) at the Institute Laue-Langevin (ILL), Grenoble, France. Beamline scientist Thilo Pirling supported us throughout and contributed to successful measurements. The marble samples were gratefully provided by Marmi Carrara s.l.r., Carrara, Italy. Anne Voigtländer was supported with a BMBF Scholarship by the Rosa-Luxemburg-Foundation. The manuscript improved by discussions with Rebecca Kühn, Frank R. Schilling, and Jens M. Turowski.

References

Alber, M., & Hauptfleisch, U. (1999). Generation and visualization of microfractures in Carrara marble for estimating fracture toughness, fracture shear and fracture normal stiffness. *International Journal of Rock Mechanics and Mining Sciences*, *36*(8), 1065–1071. https://doi.org/10.1016/S1365-1609(99)00069-6

Atkinson, B. K., & Meredith, P. G. (1987). The theory of subcritical crack growth with applications to minerals and rocks. In B. K. Atkinson (Ed.), *Fracture mechanics of rock* (pp. 111–166). London: Academic Press. https://doi.org/10.1016/B978-0-12-066266-1.50009-0

Avseth, P., Mukerji, T., Mavko, G., & Dvorkin, J. (2010). Rock-physics diagnostics of depositional texture, diagenetic alterations, and reservoir heterogeneity in high-porosity siliciclastic sediments and rocks—A review of selected models and suggested work flows. *Geophysics*, *75*(5), 75A31. https://doi.org/10.1190/1.3483770

Balestrieri, M. L., Pandeli, E., Bigazzi, G., Carosi, R., & Montomoli, C. (2011). Age and temperature constraints on metamorphism and exhumation of the syn-orogenic metamorphic complexes of Northern Apennines, Italy. *Tectonophysics*, *509*(3–4), 254–271. https://doi.org/10.1016/j.tecto.2011.06.015

Barber, D. J., Wenk, H. R., Gomez-Barreiro, J., Rybacki, E., & Dresen, G. (2007). Basal slip and texture development in calcite: New results from torsion experiments. *Physics and Chemistry of Minerals*, *34*(2), 73–84. https://doi.org/10.1007/s00269-006-0129-3

Baud, P., Zhu, W., & Wong, T. F. (2000). Failure mode and weakening effect of water on sandstone. *Journal of Geophysical Research*, *105*(B7), 16,371–16,389. https://doi.org/10.1029/2000JB900087

Bjerrum, L., & Jørstad, F. A. (1968). Stability of rock slopes in Norway. *Norwegian Geotechnical Institut*, *79*, 1–11.

Borg, I., & Handin, J. (1967). Torsion of calcite single crystals. *Journal of Geophysical Research*, *72*(2), 641–669. https://doi.org/10.1029/jz072i002p00641

Bragg, W. L. (1924). The refractive indices of calcite and aragonite. *Proceedings of the Royal Society of London*, *105*(732), 370–386.

Brantut, N., Baud, P., Heap, M. J., & Meredith, P. G. (2012). Micromechanics of brittle creep in rocks. *Journal of Geophysical Research*, *117*, B08412. https://doi.org/10.1029/2012JB009299

Brantut, N., Heap, M. J., Baud, P., & Meredith, P. G. (2014). Rate- and strain-dependent brittle deformation of rocks. *Journal of Geophysical Research: Solid Earth*, *119*, 1818–1836. https://doi.org/10.1002/2013JB010448

Brantut, N., Heap, M. J., Meredith, P. G., & Baud, P. (2013). Time-dependent cracking and brittle creep in crustal rocks: A review. *Journal of Structural Geology*, *52*, 17–43. https://doi.org/10.1016/j.jsg.2013.03.007

Bruner, W. M. (1984). Crack growth during unroofing of crustal rocks: Effects on thermoelastic behavior and near-surface stresses. *Journal of Geophysical Research*, *89*(B6), 4167–4184. Retrieved from file://localhost/Users/jescartin/WORK/Referencias/pdfs/Bruner1984.pdf

Carmignani, L., & Kligfield, R. (1990). Crustal extension in the northern Apennines: The transition from compression to extension in the Alpi Apuane core complex. *Tectonics*, *9*(6), 1275–1303. https://doi.org/10.1029/TC009i006p01275

Chen, K., Kunz, M., Tamura, N., & Wenk, H. R. (2015). Residual stress preserved in quartz from the san Andreas Fault Observatory at Depth. *Geology*, *43*(3), 219–222. https://doi.org/10.1130/G36443.1

Collins, B. D., & Stock, G. M. (2016). Rockfall triggering by thermal stressing of exfoliation fractures. *Nature Geoscience*, *9*(5), 395–400. https://doi.org/10.1038/NGEO2686

Covey-Crump, S. J., & Schofield, P. F. (2009). Neutron diffraction and the mechanical behavior of geological materials. In L. Liang, R. Rinaldi, & H. Schober (Eds.), *Neutron applications in Earth, energy and environmental sciences* (pp. 257–282). Boston, MA: Springer. https://doi.org/10.1007/978-0-387-09416-8_9

Damjanac, B., & Fairhurst, C. (2010). Evidence for a long-term strength threshold in crystalline rock. *Rock Mechanics and Rock Engineering*, *43*(5), 513–531. https://doi.org/10.1007/s00603-010-0090-9

Darling, T. W., TenCate, J. A., Brown, D. W., Clausen, B., & Vogel, S. C. (2004). Neutron diffraction study of the contribution of grain contacts to nonlinear stress-strain behavior. *Geophysical Research Letters*, *31*, L16604. https://doi.org/10.1029/2004GL020463

Davies, T. R. H., McSaveney, M. J., & Boulton, C. J. (2012). Elastic strain energy release from fragmenting grains: Effects on fault rupture. *Journal of Structural Geology*, *38*, 265–277. https://doi.org/10.1016/j.jsg.2011.11.004

De Bresser, J. H. P., & Spiers, C. J. (1997). Strength characteristics of the r, f, and c slip systems in calcite. *Tectonophysics*, *272*(1), 1–23. https://doi.org/10.1016/S0040-1951(96)00273-9

Diederichs, M. S. (2003). Rock fracture and collapse under low confinement conditions. *Rock Mechanics and Rock Engineering*, *36*(5), 339–381. https://doi.org/10.1007/s00603-003-0015-y

Eberhardt, E., Stead, D., & Stimpson, B. (1999). Quantifying progressive pre-peak brittle fracture damage in rock during uniaxial compression. *International Journal of Rock Mechanics and Mining Sciences*, *36*(3), 361–380. https://doi.org/10.1016/S0148-9062(99)00019-4

Emery, C. L. (1964). Strain energy in rocks. In W. R. Judd (Ed.), *State of stress in Earth's crust* (pp. 234–279). New York: Elsevier.

Engelder, T. (1993). *Stress regimes in the lithosphere*. Princeton: Princeton University Press.

Engelder, T., & Sbar, M. L. (1977). The relationship between in situ strain relaxation and outcrop fractures in the Potsdam sandstone, Alexandria Bay, New York. *Pure and Applied Geophysics*, *115*(1–2), 41–55. https://doi.org/10.1007/BF01637096

Engelder, T., Sbar, M. L., & Kranz, R. L. (1977). A mechanism for strain relaxation of Barre Granite: opening of microfractures. *Pure and Applied Geophysics*, *115*(1-2), 27–40. https://doi.org/10.1007/BF01637095

Eppes, M.-C., & Keanini, R. (2017). Mechanical weathering and rock erosion by climate-dependent subcritical cracking. *Reviews of Geophysics*, *55*, 470–508. https://doi.org/10.1002/2017RG000557

Friedman, M. (1972). Residual elastic strain in rocks. *Tectonophysics*, *15*(4), 297–330. https://doi.org/10.1016/0040-1951(72)90093-5

Friedman, M., & Logan, J. M. (1970). Influence of residual elastic strain on the orientation of experimental fractures in three quartzose sandstones. *Journal of Geophysical Research*, *75*(2), 387–405. https://doi.org/10.1029/JB075i002p00387

Gallagher, J. J., Friedman, M., Handin, J. W., & Sowers, G. M. (1974). Experimental studies relating to microfracture in sandstone. *Tectonophysics*, *21*(3), 203–247. https://doi.org/10.1016/0040-1951(74)90053-5

Hall, S. A., Wright, J., Pirling, T., Andò, E., Hughes, D. J., & Viggiani, G. (2011). Can intergranular force transmission be identified in sand? *Granular Matter*, *13*(3), 251–254. https://doi.org/10.1007/s10035-011-0251-x

Hashin, Z., & Shtrikman, S. (1962). A variational approach to the theory of the elastic behaviour of polycrystals. *Journal of the Mechanics and Physics of Solids*, *10*(4), 343–352. https://doi.org/10.1016/0022-5096(62)90005-4

Hill, R. (1963). Elastic properties of reinforced solids: Some theoretical principles. *Journal of the Mechanics and Physics of Solids*, *11*(5), 357–372. https://doi.org/10.1016/0022-5096(63)90036-X

Holden, T. M., Root, J. H., Holt, R. A., & Hayashi, M. (1995). Neutron-diffraction measurements of stress. *Physica B: Condensed Matter*, *213–214*(C), 793–796. https://doi.org/10.1016/0921-4526(95)00282-E

Holzhausen, G. R., & Johnson, A. M. (1979). The concept of residual stress in rock. *Tectonophysics*, *58*(3-4), 237–267. https://doi.org/10.1016/0040-1951(79)90311-1

Homola, A. M., Israelachvili, J. N., Gee, M. L., & McGuiggan, P. M. (1989). Measurements of and relation between the adhesion and friction of two surfraces separated by molecularly thin liquid films. *Journal of Tribology*, *111*(4), 675–682. https://doi.org/10.1115/1.3261994

Hoskins, E. R., & Russell, J. E. (1981). The origin of the measured residual strains in crystalline rocks. In N. L. Carter, M. Friedman, J. M. Logan, & D. W. Stearns (Eds.), *Mechanical behavior of crustal rocks: The Handin Volume, 24*, *Geophysica* (pp. 187–198). Washington, DC: American Geophysical Union. https://doi.org/10.1029/GM024p0187

Kieslinger, A. (1958). Restspannung und Entspannung im Gestein. *Geologie Und Bauwesen*, *24*(2), 95–112.

King, A., Johnson, G., Engelberg, D., Ludwig, W., & Marrow, J. (2008). Observations of intergranular stress corrosion cracking in a grain-mapped polycrystal. *Science*, *321*(5887), 382–385. https://doi.org/10.1126/science.1156211

Koch, A., & Siegesmund, S. (2004). The combined effect of moisture and temperature on the anomalous expansion behaviour of marble. *Environmental Geology*, *46*(3–4), 350–363. https://doi.org/10.1007/s00254-004-1037-9

Krautblatter, M., & Moore, J. R. (2014). Rock slope instability and erosion: Toward improved process understanding. *Earth Surface Processes and Landforms*, *39*(9), 1273–1278. https://doi.org/10.1002/esp.3578

Lawn, B. R. (1993). *Fracture of brittle solids* (2nd ed.). Cambridge: Cambridge University Press. https://doi.org/10.1017/CBO9780511623127

Lee, S. Y., Choo, H., Liaw, P. K., An, K., Hubbard, C. R., Choo, H., & Rogge, R. B. (2011). A study on fatigue crack growth behavior subjected to a single tensile overload: Part II. Transfer of stress concentration and its role in overload-induced transient crack growth. *Acta Materialia*, *59*(2), 485–494. https://doi.org/10.1016/j.actamat.2010.09.049

Luzin, V., Dmitry, N., & Siegesmund, S. (2014). Temperature induced internal stress in Carrara marble. *Materials Science Forum*, *777*, 148–154. https://doi.org/10.4028/www.scientific.net/MSF.777.148

Malkin, A. I. I. (2012). Regularities and mechanisms of the Rehbinder's effect. *Colloid Journal*, *74*(2), 223–238. https://doi.org/10.1134/S1061933X12020068

Meredith, P. G., Knight, K. S., Boon, S. A., & Wood, I. G. (2001). The microscopic origin of thermal cracking in rocks: An investigation by simultaneous time-of-flight neutron diffraction and acoustic emission monitoring. *Geophysical Research Letters*, *28*, 2105–2108. https://doi.org/10.1029/2000GL012470

Molli, G., & Heilbronner, R. (1999). Microstructures associated with static and dynamic recrystallization of Carrara marble (Alpi Apuane, NW Tuscany, Italy). *Geologie en Mijnbouw*, *78*(1), 119–126. https://doi.org/10.1023/A:1003826904858

Molli, G., Vitale Brovarone, A., Beyssac, O., & Cinquini, I. (2018). RSCM thermometry in the Alpi Apuane (NW Tuscany, Italy): New constraints for the metamorphic and tectonic history of the inner northern Apennines. *Journal of Structural Geology*, *113*, 200–216. https://doi.org/10.1016/j.jsg.2018.05.020

Müller, L. (1969). Geomechanische Auswirkungen yon Abtragungsvorgängen. *Geologische Rundschau*, *59*(1), 163–178. https://doi.org/10.1007/BF01824949

Nara, Y., Kashiwaya, K., Nishida, Y., & Ii, T. (2017). Influence of surrounding environment on subcritical crack growth in marble. *Tectonophysics*, *706-707*, 116–128. https://doi.org/10.1016/j.tecto.2017.04.008

Nichols, T. C., Jr (1975). Deformations associated with relaxation of residual stresses in a sample of Barre Granite from Vermont. *Geological Survey Professional Paper*, *875*.

Nichols, T. C. Jr., & Abel, J. F. (1975). Mobilized residual energy—A factor in rock deformation. *Bulletin of the Association of Engineering Geologists*, *12*(3), 213–225.

Nicolas, A., Fortin, J., Regnet, J. B., Dimanov, A., & Gúeguen, Y. (2016). Brittle and semi-brittle behaviours of a carbonate rock: Influence of water and temperature. *Geophysical Journal International*, *206*(1), 438–456. https://doi.org/10.1093/gji/ggw154

Noyan, I. C., & Cohen, J. B. (1987). *Residual stresses. Measurement by diffraction and interpretation*. New York, Berlin, Heidelberg, London, Paris, Tokyo: Springer.

Passchier, C. W., & Trouw, R. A. J. (2005). *Microtectonics* (2nd ed.). Berlin, Heidelberg: Springer.

Peck, L. (1983). Stress corrosion and crack propagation in Sioux quarzite. *Journal of Geophysical Research*, *88*(B6), 5037–5046. https://doi.org/10.1029/JB088iB06p05037

Pintschovius, L. (1992). Macrostresses, microstresses and stress tensors. In M. T. Hutchings, & A. D. Krawitz (Eds.), *Measurement of residual and applied stress using neutron diffraction* (NATO ASI S, pp. 115–130). Dordrecht: Kluwer Academic Publishers. https://doi.org/10.1007/978-94-011-2797-4_7

Pirling, T., Bruno, G., & Withers, P. J. (2006). SALSA—A new instrument for strain imaging in engineering materials and components. *Materials Science and Engineering*, *437*(1), 139–144. https://doi.org/10.1016/j.msea.2006.04.083

Platt, J. P., & De Bresser, J. H. P. (2017). Stress dependence of microstructures in experimentally deformed calcite. *Journal of Structural Geology*, *105*(June), 80–87. https://doi.org/10.1016/j.jsg.2017.10.012

Pollet-Villard, M., Daval, D., Ackerer, P., Saldi, G. D., Wild, B., Knauss, K. G., & Fritz, B. (2016). Does crystallographic anisotropy prevent the conventional treatment of aqueous mineral reactivity? A case study based on K-feldspar dissolution kinetics. *Geochimica et Cosmochimica Acta*, *190*, 294–308. https://doi.org/10.1016/j.gca.2016.07.007

Potyondy, D. O. (2007). Simulating stress corrosion with a bonded-particle model for rock. *International Journal of Rock Mechanics and Mining Sciences*, *44*(5), 677–691. https://doi.org/10.1016/j.ijrmms.2006.10.002

Rao, K. V. K., Naidu, S. V. N., & Murthy, K. S. (1968). Precision lattice parameters and thermal expansion of calcite. *Journal of Physics and Chemistry of Solids*, *29*(2), 245–248. https://doi.org/10.1016/0022-3697(68)90068-1

Rehbinder, P. A., & Shchukin, E. D. (1972). Surface phenomena in solids during deformation and fracture processes. *Progress in Surface Science*, *3*(2), 97–188. https://doi.org/10.1016/0079-6816(72)90011-1

Richard, D., Ferrand, M., & Kearley, G. J. (1996). Analysis and visualisation of neutron-scattering data. *Journal of Neutron Research*, *4*(1), 33–39. https://doi.org/10.1080/10238169608200065

Ritchie, R. O. (2011). The conflicts between strength and toughness. *Nature Materials*, *10*(11), 817–822. https://doi.org/10.1038/nmat3115

Sadananda, K., Solanki, K. N., & Vasudevan, A. K. (2017). Subcritical crack growth and crack tip driving forces in relation to material resistance. *Corrosion Reviews*, *35*(4–5), 251–265. https://doi.org/10.1515/corrrev-2017-0034

Savage, W. Z. (1978). The development of residual stress in cooling rock bodies. *Geophysical Research Letters*, *5*(8), 633–636. https://doi.org/10.1029/GL005i008p00633

Scheffzük, C., Siegesmund, S., & Koch, A. (2004). Strain investigations on calcite marbles using neutron time-of-flight diffraction. *Environmental Geology*, *46*(3–4), 468–476. https://doi.org/10.1007/s00254-004-1048-6

Scheffzük, C., Siegesmund, S., Nikolayev, D. I., & Hoffmann, A. (2007). Texture, spatial and orientation dependence of internal strains in marble: A key to understanding the bowing of marble panels? *Geological Society, London, Special Publications*, *271*(1), 237–249. https://doi.org/10.1144/GSL.SP.2007.271.01.23

Schofield, P. F., Covey-Crump, S. J., Daymond, M. R., Stretton, I. C., Knight, K. S., & Holloway, R. F. (2006). Methodology and recent developments for using neutron diffraction to characterize the mechanical properties of rocks. *Physica B: Condensed Matter*, *385-386*, 938–941. https://doi.org/10.1016/j.physb.2006.05.277

Schofield, P. F., Covey-Crump, S. J., Stretton, I. C., Daymond, M. R., Knight, K. S., & Holloway, R. F. (2003). Using neutron diffraction measurements to characterize the mechanical properties of polymineralic rocks. *Mineralogical Magazine*, *67*(5), 967–987. https://doi.org/10.1180/0026461036750138

Schott, J., Brantley, S. L., Crerar, D. A., Guy, C., Borcsik, M., & Willaime, C. (1989). Dissolution kinetics of strained calcite. *Geochimica et Cosmochimica Acta*, *53*(2), 373–382. https://doi.org/10.1016/0016-7037(89)90389-X

Sekine, K., & Hayashi, K. (2009). Residual stress measurements on a quartz vein: A constraint on paleostress magnitude. *Journal of Geophysical Research*, *114*, B01404. https://doi.org/10.1029/2007JB005295

Siegesmund, S., Mosch, S., Scheffzük, C., & Nikolayev, D. I. (2008). The bowing potential of granitic rocks: Rock fabrics, thermal properties and residual strain. *Environmental Geology*, *55*(7), 1437–1448. https://doi.org/10.1007/s00254-007-1094-y

Siegesmund, S., Ruedrich, J., & Koch, A. (2008). Marble bowing: Comparative studies of three different public building facades. *Environmental Geology*, *56*(3–4), 473–494. https://doi.org/10.1007/s00254-008-1307-z

Silberberg, A., & Hennenberg, M. (1984). Relaxation of stored mechanical stress along chemical reaction pathways. *Nature*, *312*(5996), 746–748. https://doi.org/10.1038/312746a0

Timoshenko, S. P., & Goodier, J. N. (1970). *Theory of elasticity* (3rd ed.). New York: McGraw-Hill Inc.

Toribio, J. (1998). Residual stress effects in stress corrosion cracking. *Journal of Materials Engineering and Performance*, *7*(2), 173–182. https://doi.org/10.1361/105994998770347891

Ungár, T. (1998). Strain broadening caused by dislocations. *Materials Science Forum*, *278-281*, 151–157. https://doi.org/10.4028/www.scientific.net/MSF.278-281.151

Varnes, D. J., & Lee, F. T. (1972). Hypothesis of mobilization of residual stress in rock. *Geological Society of America Bulletin*, *83*(September), 2863–2866. https://doi.org/10.1130/0016-7606(1972)83[2863:HOMORS]2.0.CO;2

Violay, M., Nielsen, S., Gibert, B., Spagnuolo, E., Cavallo, A., Azais, P., et al. (2014). Effect of water on the frictional behavior of cohesive rocks during earthquakes. *Geology*, *42*(1), 27–30. https://doi.org/10.1130/G34916.1

Voight, B. (1966). Residual stresses in rocks. In *Internat. Soc. Rock Mechanics Cong., 1st, Lisbon* (pp. 45–50). Bertrand: International Society for Rock Mechanics.

Voigtländer, A., Leith, K., & Krautblatter, M. (2017). Constraining the physics of subcritical crack growth in Carrara marble using neutron diffraction techniques. In *Geological Society of America Abstracts with Programs* (Vol. 49). Boulder, CO: Geological Society of America. https://doi.org/10.1130/abs/2017AM-296203

Voigtländer, A., Leith, K., & Krautblatter, M. (2018). Subcritical crack growth and progressive failure in Carrara marble under wet and dry conditions. *Journal of Geophysical Research: Solid Earth*, *123*, 3780–3798. https://doi.org/10.1029/2017JB014956

Watt, J. P., & Peselnick, L. (1980). Clarification of the Hashin-Shtrikman bounds on the effective elastic moduli of polycrystals with hexagonal, trigonal, and tetragonal symmetries. *Journal of Applied Physics*, *51*(3), 1525–1531. https://doi.org/10.1063/1.327804

Weinberger, R., Eyal, Y., & Mortimer, N. (2010). Formation of systematic joints in metamorphic rocks due to release of residual elastic strain energy, Otago schist, New Zealand. *Journal of Structural Geology*, *32*(3), 288–305. https://doi.org/10.1016/j.jsg.2009.12.003

Wheeler, J. (2018). The effects of stress on reactions in the Earth: Sometimes rather mean, usually normal, always important. *Journal of Metamorphic Geology*, *36*(4), 439–461. https://doi.org/10.1111/jmg.12299

Withers, P. J. (2007). Residual stress and its role in failure. *Reports on Progress in Physics*, *70*(12), 2211–2264. https://doi.org/10.1088/0034-4885/70/12/R04

Withers, P. J. (2015). Fracture mechanics by three-dimensional crack-tip synchrotron X-ray microscopy. *Philosophical Transactions of the Royal Society of London. Series A*, *373*(2036), 20130157. https://doi.org/10.1098/rsta.2013.0157

Withers, P. J., & Bhadeshia, H. K. D. H. (2001a). Residual stress. Part 1—Measurement techniques. *Materials Science and Technology*, *17*(4), 355–365. https://doi.org/10.1179/026708301101509980

Withers, P. J., & Bhadeshia, H. K. D. H. (2001b). Residual stress. Part 2—Nature and origins. *Materials Science and Technology*, *17*(4), 366–375. https://doi.org/10.1179/026708301101510087

Zang, A., & Berckhemer, H. (1989). Residual stress features in drill cores. *Geophysical Journal International*, *99*(3), 621–626. https://doi.org/10.1111/j.1365-246X.1989.tb02046.x

Zang, A., & Stephansson, O. (2010). *Stress field of Earth's crust*. Berlin, Heidelberg, New York: Springer. https://doi.org/10.1007/978-1-4020-8444-7